Environment regime influence on Chlorophyll-a abundance and distribution in North Indian Ocean

Thushani Suleka Madhubha Elepathage [Corresp., 1, 2], **Danling Tang** [Corresp. 1, 2]

[1] Guangdong Key Laboratory of Ocean Remote sensing, LTO, South China Sea Institute of Oceanology, Chinese Academy of Sciences, Guangzhou, Guangdong, China

[2] University of Chinese Academy of Sciences, Beijing, China

Corresponding Authors: Thushani Suleka Madhubha Elepathage, Danling Tang
Email address: thushani@scsio.ac.cn, lingzistdl@126.com

North Indian Ocean region around India and Sri Lanka is a complex and rich coastal ecosystem undergoing various seasonal and inter-annual changes and various pressures. Hence the objective of this study was to assess the scales of coupling between chlorophyll-a concentration (chl-a) and the influencing variables and explore the nature of the spatiotemporal variability of them. The seasonal and annual variations of chl-a along the Bay of Bengal (BoB), Arabian sea (AS) and ocean region around Sri Lanka in relation to the physical and chemical oceanographic variables were analyzed using satellite observations covering the period of 2002-2018. The effects of diffuse attenuation coefficient, photosynthetically available radiation (PAR), sea surface temperature (SST), Wind speed, Eastward wind component, Nitrate, Black carbon column mass density, Sea Salt Surface Mass Concentration, Open water net downward longwave flux, Surface emissivity were considered on a monthly time scale. Wavelet analysis and the Boosted Regression Trees (BRT) were used as the main analysis and modeling methods. The peaks of chl-a, diffuse attenuation coefficient, and nitrate were observed in September. In wind speed and eastward wind it was July and in black carbon column mass density, and PAR in March. In Sea Salt Surface Mass Concentration, Open water net downward longwave flux, Surface emissivity, Diffuse attenuation coefficient for downwelling irradiance, and SST mean maximums were found in June, February, November, September, April respectively. In BRT model the estimated cross validation (cv) deviance, standard error (se), training data correlation, cv correlation, and D^2 were 0.003, 0.002, 0.932, 0.949, and 0.846 respectively. According to the results, diffuse attenuation coefficient (90%), eastward wind component (3.7%) and nitrate (3%) were the most positively correlated variables with Chl-a occurrence. SST evidenced an inverse relationship with Chl-a. According to the model built <42 Einsteinm^{-2}day^{-1} PAR, <0.986 surface emissivity, <70 Wm^{-2} open water net downward

long wave flux, 28.2 -28.5 ^{0}C SST , 2 ms^{-1} Wind speed, 5 ms^{-1} - 6 ms^{-1} eastward wind, 4.8 $x10^{-8}$ -$7x10^{-8}$ kgm^{-3} sea salt surface mass concentration, and 0.1-0.5micromoleL^{-1} nitrate are favourable for the optimum level of phytoplankton occurrence. Since BRT deals robustly with non-linear relationships of the environmental variables it can be used in further studies of ecological modeling.

Environment regime influence on Chlorophyll-a abundance and distribution in North Indian Ocean

Thushani Suleka Madhubhashini Elepathage, Danling TANG

LTO, Guangdong Key Laboratory of Ocean Remote Sensing, South China Sea Institute of Oceanology, Chinese Academy of Sciences, Guangzhou, China; University of Chinese Academy of Sciences, Beijing 100049, China

Corresponding Author:
Thushani Suleka Madhubhashini Elepathage
Room no 1502, Building no 2, 164, West Xingang Road, South China Sea Institute of Oceanology, Guangzhou, China, 510301
Email address: thushani@scsio.ac.cn

Danling TANG
Room no 1603B, Building no 2, 164, West Xingang Road, South China Sea Institute of Oceanology, Guangzhou, China, 510301
Email address: lingzistdl@126.com

Abstract

North Indian Ocean region around India and Sri Lanka is a complex and rich coastal ecosystem undergoing various seasonal and inter-annual changes and various pressures. Hence the objective

of this study was to assess the scales of coupling between chlorophyll-a concentration (chl-a) and the influencing variables and explore the nature of the spatiotemporal variability of them. The seasonal and annual variations of chl-a along the Bay of Bengal (BoB), Arabian sea (AS) and ocean region around Sri Lanka in relation to the physical and chemical oceanographic variables were analyzed using satellite observations covering the period of 2002-2018. The effects of diffuse attenuation coefficient, photosynthetically available radiation (PAR), sea surface temperature (SST), Wind speed, Eastward wind component, Nitrate, Black carbon column mass density, Sea Salt Surface Mass Concentration, Open water net downward longwave flux, Surface emissivity were considered on a monthly time scale. Wavelet analysis and the Boosted Regression Trees (BRT) were used as the main analysis and modeling methods. The peaks of chl-a, diffuse attenuation coefficient, and nitrate were observed in September. In wind speed and eastward wind it was July and in black carbon column mass density, and PAR in March. In Sea Salt Surface Mass Concentration, Open water net downward longwave flux, Surface emissivity, Diffuse attenuation coefficient for downwelling irradiance, and SST mean maximums were found in June, February, November, September, April respectively. In BRT model the estimated cross validation (cv) deviance, standard error (se), training data correlation, cv correlation, and D^2 were 0.003, 0.002, 0.932, 0.949, and 0.846 respectively. According to the results, diffuse attenuation coefficient (90%), eastward wind component (3.7%) and nitrate (3%) were the most positively correlated variables with Chl-a occurrence. SST evidenced an inverse relationship with Chl-a. According to the model built <42 Einsteinm^{-2}day^{-1} PAR, <0.986 surface emissivity, <70 Wm^{-2} open water net downward long wave flux, 28.2 -28.5 ^{0}C SST , 2 ms^{-1} Wind speed, 5 ms^{-1} - 6 ms^{-1} eastward wind, 4.8 x10^{-8} -7x10^{-8} kgm^{-3} sea salt surface mass concentration, and 0.1-0.5micromoleL^{-1} nitrate are favourable for the optimum level of phytoplankton occurrence. Since

47 BRT deals robustly with non-linear relationships of the environmental variables it can be used in
48 further studies of ecological modeling.
49
50 Key words: Wavelet analysis, Boosted Regression Trees, Bay of Bengal, Arabian Sea, Sri lanka
51 Exclusive Economic Zone, Phytoplankton, Monsoon, Upwelling, Predictor variables, Seasonal
52

53 Introduction

54 Arabian Sea (AS), Bay of Bengal (BoB) and Sri Lankan Exclusive economic zone (EEZ) are
55 parts of North Indian Ocean which surround India and Sri Lanka. India has approximately 6000
56 km long coastline and Sri Lanka 1,620 km (Dey & Singh, 2003; Government of Sri Lanka,
57 Ministry of Finance, National Agency for, & Public Private Partnership, 2018). These oceanic
58 regions which are close to the coastlines and equator experience many physical and chemical
59 dynamics that effect to the primary production in the region (Krishna et al., 2015; Strutton et al.,
60 2015). Studying the circulation dynamics and the biological processes are important in
61 understanding the numerous ocean processes. In the ocean, the physical, chemical, and biological
62 processes are interlinked (Danling Tang, Kawamura, & Luis, 2002). Ocean properties such as
63 chlorophyll concentration, currents, sea surface temperature, suspended particulate matter,
64 dissolved organic matter ocean, ENSO event, fronts, and eddies influence the ocean dynamics.
65 Remote sensing data provide information on the properties of ocean (Eg: concentration of
66 phytoplankton pigments, suspended sediments, temperature, and radiation) and they can be used
67 to monitor these processes in large special areas for long terms (Elepathage & Tang, 2018;
68 Elepathage, Tang, & Wang, 2018; D. L. Tang, Kawamura, & Luis, 2002; DanLing. Tang & Pan,
69 2011).

Although some studies have been done regarding the chlorophyll distributions in reference to the sea surface temperature, nitrate, sea surface height and mixed layer depth in either Arabian Sea or Bay of Bengal (Narvekar & Kumar, 2014; Sarangi & Devi, 2017; Sathyendranath, Gouveia, Shetye, Ravindran, & Platt, 1991), very limited efforts have been given to study all the factors that affect the chlorophyll distribution in the whole region. Especially not enough studies have been carried out in Sri Lankan region. AS is a highly productive area than the BoB (Jana et al., 2018). The continental shelf of the AS is much shallower compared to the shelf in the southern BoB. AS is bounded to the east by India, to the north by Pakistan, Iran, and Saudi Arabia, and to the west by Oman and Somalia. The Arabian Sea is located in the monsoon region, hence nutrient cycle is affected by the monsoonal events (Karuppasamy, Muraleedharan, Dineshkumar, & Nair, 2010). The northern BoB is much productive than southern part since North region feeds from Ganges-Brahmaputra delta (Chauhan, Nagur, Mohan, Nayak, & Navalgund, 2001). The BoB circulation is affected by both wind and river forcing (Cutler & Swallow, 1984; Durand et al., 2011). In spring and autumn, the seasonally reversing wind force create reversing boundary currents and opposing gyre circulations (Cutler & Swallow, 1984).

Sri Lankan ocean region is also affected by the monsoon and hence the primary production is changed with the monsoon. The Indian Ocean monsoon currents flow eastwards along South region of Sri Lanka during the summer (May to September). They are called Summer Monsoon Current (SMC) or South-West monsoon currents. In winter or dry season from December to March, they start to flow westward and they are called Winter Monsoon Current (WMC) or North-East monsoon currents (Schott & McCreary, 2001). The SMC plays an important role in transferring of more saline water from the AS to the BoB (Jensen, 2001; Vinayachandran, Murty, & Ramesh Babu, 2002). They are linked with the remote forcing by the wind, as well as

93 interactions with westward-propagating Rossby waves and eddies (Rath, Vinaychandran, Behara,
94 & Neema, 2017).

95 These areas are interlinked by the ocean physical dynamics and hence the phytoplankton density
96 that affects directly for the biodiversity and fisheries are changed with these influencing factors
97 (Strutton et al., 2015). Phytoplankton community is the base of the ocean food web. Hence it
98 plays a major role in regulating ocean biodiversity (Kong et al., 2019). The objective of this
99 paper is to study the variability of the chlorophyll concentrations in the discussed part of North
100 Indian Ocean in order to discuss the distribution, seasonal changes and to model the chlorophyll
101 abundance after identifying the influencing factors regulate the chlorophyll concentrations.

102 Materials & Methods

103 Study area and Data Set

104 The study area (Figure 1) lies between 72^0 E, 0^0N and 98.5^0E, 22^0N which consists of BoB, AS
105 and Sri Lankan EEZ was used for this study. The remote sensing data of Chl-a, diffuse
106 attenuation coefficient, eastward surface wind, surface emissivity, wind speed, sea salt surface
107 mass concentration, black carbon column mass density, open water net downward longwave
108 radiation, and organic carbon column mass density from 2002 to 2018 and nitrates from 1998 to
109 2018 were analysed since they were found to be interlinked according to the previous studies we
110 have done and according to the literature review.

111 Inter-annual time series Chl-a concentration data in the unit of mg m^{-3}, Sea Surface Temperature
112 (SST) at 4 microns data in ^{0}C, diffuse attenuation coefficient for downwelling irradiance at 490
113 nm (KD_490) in m^{-1} and Photosynthetically Available Radiation (PAR) in Einstein m^{-2} day^{-1}
114 (4km resolution) were obtained from Moderate-resolution Imaging Spectroradiometer (MODIS)-

Aqua MODISA_L3m. Nitrate data 0.67 x 1.25 deg. data in micromole/L were taken from NASA Ocean Biogeochemical Model (NOBM). Sea Salt Surface Mass Concentration in kg m^{-3}, black Carbon Column Mass Density in kg m^{-2}, eastward wind component @1000hPa in ms^{-1}, open water net downward longwave flux in W m^{-2} and surface emissivity 0.5 x 0.625 deg data were obtained from Modern-Era Retrospective analysis for Research and Applications, Version 2 (MERRA-2) Model M2TMNXRAD v5.12.4. Near-surface wind speed 0.25 deg. data in ms-1 were obtained from the Global Land Data Assimilation System (GLDAS) Model GLDAS_NOAH025_M v2.1. These data were obtained from https://giovanni.gsfc.nasa.gov/giovanni.

Methods

Preliminary analysis

The most common way of expressing the temporal variability of a data set is through monthly mean line graphs (Figure 2). Analytically, means and dispersion metrics were calculated from the 17 years of data logs. The standard deviations among them are mentioned in Table 1.

Wavelet Coherence Analysis

The spatial and temporal patterns in the time series data reflect important parts of the biological cycles, particularly at intra-annual time scales. Wavelet analysis is a suitable method to examine the localized patterns of environment changes (Cyriac, Ghoshal, Shaileshbhai, & Chakraborty, 2016; Lumban-Gaol et al., 2015; Torrence & Compo, 1998).

The wavelet transform can be used to investigate the time series features at local scales with the broad features at long time scales and fine features at short ones (Carey et al., 2013). This is useful in analyzing the time series data with non-stationary power at many different frequencies (Daubechies, 1990). In this study to assess correlation and coupling between the influence

variables and Chl-a, the co-variation of the power spectra of those variables (Figure 3) were calculated using the wavelet coherence using R 3.4.2.

The wavelet power spectra are calculated in this method using the Morlet wavelet. This has been applied in many environmental studied due to since it detects time-dependent amplitude and different frequencies' phases in the time series (Torrence & Compo, 1998).

For a time series *Xn*, an ex- wave modulated by a Gaussian is characterized as:

$$\Psi_0(\eta) = \pi^{-\frac{1}{4}} e^{i\omega_0\eta} e^{-\frac{\eta^2}{2}}$$

where $\Psi_0(\eta)$ is the wavelet function, η is a dimensionless time parameter, i is an imaginary unit, and ω_0 dimensionless angular frequency. The term "wavelet function" is refers to either orthogonal or nonorthogonal wavelets. The term "wavelet basis" is used only to an orthogonal set of functions. The orthogonal basis implies discrete wavelet transform while nonorthogonal wavelet function is used for discrete or continuous wavelet transform (Farge, 1992). The wavelet function is mathematically represented for a time series *Xn* as:

$$W_n(s) = \frac{1}{N}\sum_{n'=0}^{N-1} x_{n'} \Psi * \left[\frac{(n' - \eta)\Delta t}{s}\right]$$

where (*) the complex conjugate. By varying the *s* wavelet scale and translocating along the localized time index *n* the amplitude of the studied feature vs scale and temporal change of the amplitude is graphically represented in wavelet analysis. In this equation $W_n(s)$ is the wavelet transform coefficients, Ψ is the normalized wavelet, *n* is the localized time index, and n' is the translated time index of the time ordinate *x*.

The wavelet coherence is the square of the cross-spectrum normalized by the power spectra. Wavelet coherence and phase are parts of the Fourier analysis and they quantify the cross-correlation between two time series as a function of frequency (Torrence & Compo, 1998).

The wavelet coherence of two time series X and Y analogous to the correlation coefficient in the frequency domain with wavelet transforms $W_n^X(s)$ and $W_n^Y(s)$ is mathematically written as

$$R_n^2(s) = \frac{\left|S(s^{-1}W_n^{XY}(s))\right|^2}{S\left(s^{-1}\left|W_n^X(s)\right|^2\right) \times S\left(s^{-1}\left|W_n^Y(s)\right|^2\right)}$$

Where S is a smoothing operator both in the scale axis and time domain.

$$S(W) = S_{scale}(S_{time}W_n(s)))$$

Where S_{time} smooths along the time axis and S_{scale}along the scale axis. The first-order autoregressive null model was computed via Monte Carlo approach (Maraun & Kurths, 2004; Torrence & Compo, 1998)

Boosted regression trees model execution

We modeled the occurrence and abundance of chl-a and its predictor variables using Boosted Regression Trees (BRT). Recent work has revealed that BRT is dealing well in ecological variables which have with non-linear relationships (Elith et al., 2006; J. Friedman, Hastie, & Tibshirani, 2002; Kraemer, Mehner, & Adrian, 2017; Nieto & Mélin, 2017).

Fist to determine the interannual relationship between chl-a and environment variables we used non-parametric Kendall's rank correlation (Table 2) (Kendall, 1938). Then the relationship between the chl-a (dependent variable), and physical oceanographic variables were computed by a Boosted Regression Tree (BRT) analysis with year and month as time factors. BRT modeling

can fit complex nonlinear relationships and automatically handle outliers and interaction effects between predictors (Elith & Leathwick, 2017).

An initial set of BRT models was derived at the level of individual cells to account for the heterogeneity. The BRT construction was performed using the "dismo" package (Elith & Leathwick, 2017) in R version 3.4.2 (R Development Core Team, 2017). BRT model with 0.05 learning rates and 5 levels of tree complexity 1300 trees was selected as the definitive model (Figure 4). To quantify how well the BRT model fitted the data, the percentage of deviance explained was used. The pseudo determination coefficient (D^2) (Mateo & Hanselman, 2014), was calculated with the formula:

$$D^2 = 1 - (residual\ deviance/total\ deviance)$$

Based on the result of the BRT model, the relative influence of each predictor on Chl-a was computed. The percentage of relative influence was used to quantify the importance of predictors (Figure 5). High relative influence values corresponding to the strong influence on the response (Elith & Leathwick, 2017). The partial dependency plots and weighted mean of fitted values in relation to each non-factor predictor plots were used to analyze the effect of variations in the predictors on the response variable.

Results

Preliminary analysis

According to the plots in Figure 2 surface emissivity, diffuse attenuation coefficient, and nitrate follow the same temporal variation of Chl-a. PAR, SST, and black carbon column mass density demonstrate inverse relationships with Chl. The peaks of chl-a, diffuse attenuation coefficient, and nitrate were observed in September. In wind speed and eastward wind it was July and in

black carbon column mass density, and PAR in March. In Sea Salt Surface Mass Concentration, Open water net downward longwave flux, Surface emissivity, Diffuse attenuation coefficient for downwelling irradiance, and SST mean maximums were found in June, February, November, September, April respectively.

Comparatively high standard deviations could be observed only in some months of PAR, nitrate, open water net downward longwave flux and the eastward component data. In other variables, the standard deviations among the data were generally lower than 1 (Table 1). According to Kendall's rank correlation (Table 2) only diffuse attenuation coefficient, eastward wind component, nitrate, sea salt surface mass concentration, open water net downward longwave flux, surface emissivity manifested significant relationship with Chl-a. However, this can only identify more linear relationships.

Wavelet analysis

The chl-a and the influential variables wavelet coherencies (Figure 3) can be used to interpret at what period does coherency occur between the Chl-a and predictor variables. Diffuse attenuation coefficient shows a strong coherency evidenced by the large areas with dar that do show significant coherence. The right arrows further support that they have an in-phase relationship. From around 2016 the relationship has been strengthened drastically.

SST shows a relationship with Chl in 4-8 and 8-16 periods. The strongest relationship can be seen between 8-16 period. Within the 8-16 period we can see a 135^0 phase angle of arrows. In SST also we can observe the highest relationship after 2016.

With PAR the relationship is completely out phase and after 2016 the coherence power has been increased. With wind speed, eastward surface wind component and the sea salt surface mass concentration the phase angle is 90^0 and as before the high power coherence is there after 2016.

Black carbon column mass density has a 225^0 angle and open water net downward longwave flux has a 45^0 phase angle. Surface emissivity has a 315^0 phase angle. Nitrate has an in phase coherence and unlike all others, it has the high power coherence from 2002 to 2007.

Boosted regression trees

After making several preliminary fittings as the final fitting of BRT, a 1300 trees model was selected with 0.05 learning rates and 5 levels of tree complexity. The mean total deviance of the model was 0.013, mean residual deviance was 0.002. The estimated cv deviance was 0.003 and the standard error (se) was 0.002 Training data correlation was 0.932 and cv correlation was 0.949. D^2 was 0.846. The model plot is indicated in Figure 4. Deviance was calculated from models fitted to a data set of 12 variables.

The tree complexity (TC) reflect the true interaction order in the response being modeled (Jerome H Friedman, 1999), and the best set with independent data. In Figure 4 the solid black curve is the mean, and the dotted curves are indicated in about 1 standard error area. The red line shows the minimum of the mean, and the green line the number of trees at which that occurs. Predictive performance is influenced strongly by sample size and large samples gave models with a lower predictive error.

The summary of the Model gives a feature importance plot **(**Figure 5**)**. According to Figure 5, it is clear that the diffuse attenuation coefficient is the most important variable and the month is the least important variable.

Partial dependence plots for the BRT are displayed in Figure 6. Each plot shows the relationship of chl-a (response variable) to each individual variable after accounting for the effects of all the predictor variables in the final model. Visualization of fitted functions in a BRT model is easily achieved using partial dependence functions that show the effect of a variable on the response after accounting for the average effects of all other variables in the model.

In the weighted mean of fitted values in relation to each non-factor predictor (Figure 7), the slopes of the relationships between Chl and influenced variables differed significantly across the variables. The final BRT model had 12 predictors with the two factors of year and month. Chl with the most predictive power included diffuse attenuation coefficient (90%), Eastward wind component (3.7%) and nitrate (3%). If there are strong interactions in the data or predictors are strongly correlated, they provide a useful basis for interpretation (J. H. Friedman, 2001). The diffuse attenuation coefficient and the nitrate the slope of the relationship were substantially high, whereas slopes in other variables were substantially low. The predictive accuracy of the models also varied across the variables.

These plots in Figure 8 simply show the relation between the variables in the x-axis and the mapping function f(x) on the y-axis. Plots show that diffuse attenuation coefficient, eastward wind component, and sea salt surface mass concentration are positively correlated with the response Chl-a, whereas PAR is negatively correlated. Others relationships are complex. According to the variability of Chl with other variables diffuse attenuation coefficient increases 0.1-0.6m^{-1} with primary production and then it becomes stable. PAR <42Einstein m^{-2} day^{-1}, surface emissivity <0.986 and Open water net downward longwave flux <70 Wm^{-2} is favorable for primary production. Chl-a increases with SST 28.2 -28.5 ^{0}C and then it declines. Chl-a increases at wind speed 2 ms^{-1} then stabilize and drop again at 2.8 ms^{-1}. Moreover, phytoplankton increases from the eastward wind component at 5 ms^{-1} and stabilizes at 6 ms^{-1}. Moreover, Chl-a increases at sea salt surface mass concentration from 4.8 $x10^{-8}$ to $7x10^{-8}$ kgm^{-3} and then drops. Nitrate 0.1-0.5micromoleL^{-1} is favorable for the phytoplankton abundance.

The seasonal spatiotemporal pattern of the Chl and influencing variables change (Figure 9) clearly interpret their relationships. Specially in the season from June- August the comparatively cold SST, moderate open water longwave flux, eastward wind component and nitrate show high Chl abundance and distribution. The diffuse attenuation coefficient is always following the same spatiotemporal variation pattern of Chl

Discussion

According to the results, it was clear that Chl-a and the diffuse attenuation coefficient have a positively related strong coherence. Light attenuation in an aquatic environment is the sum of light absorbing and scattering of optically active components available in water. These components include phytoplankton pigments such as chlorophyll, pure water and tripton (non pigmented particulate matter), and colored dissolved organic matter (CDOM) (Kirk, 1994). The diffuse attenuation coefficient is a key parameter used to quantify the feedback of phytoplankton biomass in the ocean (Jerlov, 1976; Kirk, 1994, 2011). Differences in phytoplankton biomass are correlated with changes in water transparency. Therefore, Diffuse attenuation of photosynthetic active radiation ($Kd_{(PAR)}$) (can be determined by Chl-a concentration (transformed as $t(x) = \ln(x+1)$) and light distribution measurements (Vernet et al., 2012).

Since the SST showed a greater value than $\pi/2$ in the wavelet coherence phase relationship, it is proven that the SST has a negative relationship with the chlorophyll. SST regulates vertical mixing and it affects the SST change in return (Kumar, Prakash, Ravichandran, & Narayana, 2016; Luis & Kawamura, 2004). Significant correlation between Chl-a concentration and SST has been found in the North Indian ocean by previous studies and they have identified that the vertical mixing of deeper water with the surface water causes a decrease in SST and supplies nutrients to the upper layers which enhance the productivity (Prakash & Ramesh, 2007). Several previous studies also have found that cold SST anomalies induce by Ekman pumping (Kug & Kang, 2006). (Weisberg & Wang, 1997) have stated that El Niño–related anomalous convection make a pair of off-equatorial cyclones with westerly wind anomalies on the equator in the equatorial central Pacific and these equatorial westerly winds deepen thermocline and raise SST giving a positive feedback for anomaly growth. (Kong et al., 2019) has found that the El Niño induces the elevated SST and SLA and increased rainfall in the open seas of the equatorial Pacific and the central southern Indian Ocean which strengthens the ocean stratification and deepens the thermocline. That leads to the reduction of mixing efficiency and inhibited vertical nutrient inputs into the euphotic

layer. Moreover, it reduces the solar radiation resulted in decreased phytoplankton production. Chl-a is anomalously negative in concert with sensitive responses to ENSO (Kong et al., 2019).

To the best of our knowledge PAR has not shown any negative relationship with chlorophyll in previous studies. Hence, it is necessary to find the reason for this relationship between PAR and Chl.

In this study, we found that wind plays a major role in regulating the air-sea interactions. Wavelet analysis clearly demonstrates that wind speed has a positive relationship with Chl-a within the study region. Vertical mixing occurs with increased wind speed cools the water and deepen the surface mixed layer transferring nutrients from deep water to the surface (Kumar et al., 2016). Moreover, since the phase angle is 90^0 upward it is clear that Chl-a is leading the wind speed, eastward component, and sea salt surface mass concentration. Wind speed governs the upwelling and vertical mixing in the upper ocean (Kumar et al., 2016). (Feng et al., 2015) has found that in low-latitude oceans and bell shaped in temperate oceans chl-a and wind speed have positive correlations. Some studies evidence that chl-a pulses are associated with the intensification of eastward winds at the surface and eastward currents in the mixed layer (Strutton et al., 2015). It is believed that the equatorial Indian Ocean is strongly influenced by physical processes on intra-seasonal to inter-annual timescales. (Waliser, Murtugudde, Strutton, & Li, 2005) have found that Chlorophyll-a can vary at Madden– Julian Oscillation (MJO) time scales. MJO is an *eastward moving* strong contributor to various extreme events of rainfall, winds, clouds, and pressure that traverses in the tropics (Drushka et al., 2012; Valadão, Carvalho, Lucio, & Chaves, 2017). The is found to be influenced by the atmospheric variability, with periods of 30–60 days and eastward propagation of atmospheric convection cells (Hendon & Salby, 1994). All of these physical processes affect the biogeochemistry of the ocean (Strutton et al., 2015). Some studies that have been carried out with satellite derived data have found that the Indian Ocean Dipole events significantly increase chl-a concentrations and primary production in eastern Indian Ocean equatorial waters, and they can also influence chl and production over the entire northern basin (Wiggert, Murtugudde, & Christian, 2006).

Ocean salinity plays a significant role in global climate variability and ocean dynamics regulation (Lagerloef, 2002). Sea surface salinity (SSS) is regulated by the local evaporation (*E*) and precipitation (*P*) in the global ocean and the river discharges in the coastal regions. In the tropical Indian Ocean (TIO), the surface salinity shows significant east-west contrast. Basically, the east-west contrast occurs because of the extreme evaporation in the Arabian Sea and abundant rainfall and river discharges in the Bay of Bengal and the eastern TIO (Schott, Dengler, & Schoenefeldt, 2002), while the SSS tongues are influenced by ocean circulations (W. Han & McCreary, 2001). Previous studied have found that the significant change in salinity appears south of the equatorial Indian Ocean with upwelling Rossby wave and high Chl-a implies high-salinity water at the surface coming from the subsurface, bringing in high nutrients or higher subsurface Chl-a (Du & Zhang, 2015). Moreover according to that study upwelling brings more significant effects on sea surface salt mass concentration than downwelling does, due to the stratification. It mainly happens due to the characteristics of the mixed layer. When upwelled high-salinity water entered the surface layer, mixing made water properties uniform in the vertical quickly (Du & Zhang, 2015) bringing the nutrients to the surface needed for the phytoplankton growth.

In this study, it is clear that nitrates have a strong positive inphase relationship with Chl-a. It is a well-known fact that nutrients such as nitrogen are essential for phytoplankton growth (Harrison, 1992). Nitrate, the most common oxidized form of nitrogen, and it provides the largest inorganic oceanic reservoir of this limiting nutrient for most marine phytoplankton (Levitus, Conkright, Reid, Najjar, & Mantyla, 1993)

We found that black carbon column mass density has a negative relationship with Chl-a. By lowering carbonate ion levels and increasing carbonate solubility, ocean acidification is thought to increase the energetic cost of calcification (Fabry, Seibel, Feely, & Orr, 2008). Acidification, therefore, could have major impacts on biogenic habitat and planetary geochemical cycles (e.g., pelagic coccolithophore algae) (Scott C. Doney et al., 2012).

Open water net downward longwave radiation flux has a positive relationship with Chl. Direct measurements of long-wave radiation fluxes are not studied with canopy and climatological studies much. The constituent downwelling (Ld) and upwelling (Lu) fluxes, or even the net flux (Ln) have also been measured only rarely (Gilgen, Ohmura, Gilgen, & Ohmura, 1999; Kessler & Jaeger, 1999).

The paucity of reliable data on long-wave radiation prevents adequate confirmation of the existing within vegetation long-wave radiation models (Paw U, 1992; Rotenberg et al., 1998). Long-wave radiation's net value (Ln) is estimated as the difference between global net radiation and the net shortwave radiation. However, the effect of longwave net downwelling radiation flux on chlorophyll has not been studied in detail yet. Previous studies also suggest that there is, an increasing need that there is a need for a good description of the temporal and spatial variation of radiation fluxes in plant canopies if processes such as photosynthesis are to be modeled successfully (Barradas, Jones, & Clark, 1999). Moreover, previous studies suggest that more attention needs to be paid to the monitoring of the long-wave radiation fluxes of different types of surfaces and in different climatic regions than is the case at present. They also mention that it will take a long time before measurements at a single site can reveal the influence of increasing CO_2 concentration in the atmosphere on long-wave counter radiation A (Kessler & Jaeger, 1999).

Model development for chlorophyll

Booster Regression Trees (BRT) seems a good choice for a chl-a model because BRT can deal with many relationships between Chl-a and the influencing factors derived from satellite data (L. Han, Rundquist, Liu, Fraser, & Schalles, 1994; Kutser, Herlevi, Kallio, & Arst, 2001). BRT is a machine-learning algorithm based on decision trees that have significant potential to analyze the remote sensing hydrological parameters. BRT uses usually thousands of decision trees to minimize model deviance (Jerome H Friedman, 1999). Each decision tree is built to minimize the error. The final BRT model is the sum of predictions of all nodes and trees. Regression models are built individually for each subsample. Since the subsamples are classified step by step using different predictors in BRT, the interactions of

predictors can be modeled. Like other decision tree algorithms, BRT simulates both non-linear and linear relationships without the requirement of data distribution (e.g. normal distribution) (Lin, Qi, Jones, & Stevenson, 2018).

The final model that is returned in the model object is built on the full data set, using the number of trees identified as optimal. BRT results clarified the influence of predictor variables on Chl-a variability, and certainly, they could provide a view of the behavior between Chl-a and physical environment, and optimal environment for the phytoplankton. From the BRT analysis, it appeared that the relative influence of each physical predictor varied between systems. According to the final model upwelling conditions with Low PAR, surface emissivity, moderate SST, wind speed and eastward wind component, open water longwave flux, sea salt surface mass concentration, nitrate are good for the phytoplankton growth. The model with the diffuse attenuation coefficient, eastward wind component, nitrate, open water net downward longwave radiation and SST were identified as the model with the highest correlation and lowest deviance and standard error.

This study presented an overview of the relationships existing between the physical environment and Chl, prominence the main features of the NIO as well as its complexity. It focused on the seasonal variations characterizing the NIO basin system. The relationships might tell us what possible evolutions are in store for phytoplankton as the physical environment is affected by climate change.

Conclusions

The overall goal of this paper was to explore the nature of the spatiotemporal variability of the studied variables and assess the scales of coupling between Chl-a and the influencing variables. Maximum abundance of Chl-a within the study area can be observed from June- September. According to the wavelet analysis and BRT, we found diffuse attenuation coefficient, eastward wind component and nitrate as the most positively correlated variables with Chl-a occurrence.

SST evidenced an inverse relationship with Chl-a. According to the model built we believe that <42Einsteinm^{-2}day^{-1} PAR, <0.986 surface emissivity, <70 Wm^{-2} open water net downward longwave flux, 28.2 -28.5 ^{0}C SST , 2 ms^{-1} Wind speed, 5 ms^{-1} - 6 ms^{-1} eastward wind, 4.8 x10^{-8} - 7x10^{-8} kgm^{-3} sea salt surface mass concentration, and 0.1-0.5micromoleL^{-1} nitrate are favorable for the optimum level of phytoplankton occurrence. Wavelet analysis and BRT deal well with the non-linear relationships of the ecological variables. Hence these methods can be used for the ecological model building in the future studies.

Acknowledgments

This study is supported by project award to DL Tang: National Natural Sciences Foundation of China (41430968, 41876136), Collaborative Innovation Center for 21st-Century Maritime Silk Road Studies, Guangzhou, China （2015HS05), and the Ph.D. scholarship of T.S.M. Elepathage provided by Chinese scholarship council. This document was produced with the financial support of the Prince Albert II of Monaco Foundation. The contents of this document are solely the liability of Ms. Thushani Suleka Madhubhashini Elepathage and under no circumstances may be considered as a reflection of the position of the Prince Albert II of Monaco Foundation and/or the IPCC. We also acknowledge the MODIS mission scientists and associated NASA personnel for the production of the data used in this research effort.

References

Barradas, V. L., Jones, H. G., & Clark, J. A. (1999). Leaf orientation and distribution in a Phaseolus vulgaris L. crop and their relation to light microclimate. *International Journal of Biometeorology*, *43*(2), 64–70. https://doi.org/10.1007/s004840050117

Carey, S. K., Tetzlaff, D., Buttle, J., Laudon, H., McDonnell, J., McGuire, K., … Shanley, J.

(2013). Use of color maps and wavelet coherence to discern seasonal and interannual climate influences on streamflow variability in northern catchments. *Water Resources Research*, *49*(10), 6194–6207. https://doi.org/10.1002/wrcr.20469

Chauhan, P., Nagur, C. R. C., Mohan, M., Nayak, S. R., & Navalgund, R. R. (2001). Surface chlorophyll-a distribution in Arabian Sea and Bay of Bengal using IRS-P4 Ocean Colour Monitor satellite data. *Current Science*, *80*(2), 127–129. https://doi.org/10.2307/24104270

Cutler, A. N., & Swallow, J. C. (1984). Surface currents of the Indian Ocean (to 25S, 100E): compiled from historical data archived by the Meteorological Office, Bracknell, UK. Retrieved from https://eprints.soton.ac.uk/14603/

Cyriac, A., Ghoshal, T., Shaileshbhai, P. R., & Chakraborty, A. (2016). Variability of sensible heat flux over the Bay of Bengal and its connection to Indian Ocean Dipole events. *Ocean Science Journal*, *51*(1), 97–107. https://doi.org/10.1007/s12601-016-0009-9

Daubechies, I. (1990). The wavelet transform, time-frequency localization and signal analysis. *IEEE Transactions on Information Theory*, *36*(5), 961–1005. https://doi.org/10.1109/18.57199

Dey, S., & Singh, R. P. (2003). Comparison of chlorophyll distributions in the northeastern Arabian Sea and southern Bay of Bengal using IRS-P4 Ocean Color Monitor data. *Remote Sensing of Environment*, *85*, 424–428. https://doi.org/10.1016/S0034-4257(03)00025-7

Drushka, K., Sprintall, J., Gille, S. T., Wijffels, S., Drushka, K., Sprintall, J., … Wijffels, S. (2012). In Situ Observations of Madden–Julian Oscillation Mixed Layer Dynamics in the Indian and Western Pacific Oceans. *Journal of Climate*, *25*(7), 2306–2328. https://doi.org/10.1175/JCLI-D-11-00203.1

Du, Y., & Zhang, Y. (2015). Satellite and Argo Observed Surface Salinity Variations in the

438 Tropical Indian Ocean and Their Association with the Indian Ocean Dipole Mode. *Journal*
439 *of Climate*, *28*(2), 695–713. https://doi.org/10.1175/JCLI-D-14-00435.1
440 Durand, F., Papa, F., Rahman, A., Bala, S. K., Durand, F., Papa, F., … Kumar Bala, S. (2011).
441 Impact of Ganges-Brahmaputra interannual discharge variations on Bay of Bengal salinity
442 and temperature during 1992-1999 period. *Journal of Earth System Science, Indian*
443 *Academy of Sciences*, *120*(5), 859–872. Retrieved from https://hal.archives-ouvertes.fr/hal-
444 00990995
445 Elepathage, T. S. M., & Tang, D. (2018). Oceanography & Marine Biology Hydro-climatic
446 variations analysis with remote sensing data on Sri Lankan ocean waters. *Journal of Marine*
447 *Biology & Oceanography*, *7*. https://doi.org/10.4172/2324-8661-C2-015
448 Elepathage, T. S. M., Tang, D., & Wang, S. (2018). Abundance of Marlins in relation to sea
449 surface temperature in Sri Lankan ocean. *Journal of Nanjing University of Information*
450 *Science & Technology(Natural Science Edition)*, (10).
451 https://doi.org/10.13878/j.cnki.jnuist.2018.03.001
452 Elith, J., Graham, C. H., Anderson, R. P., Dudík, M., Ferrier, S., Guisan, A., … HGraham, C.
453 (2006). *Novel methods improve prediction of species' distributions from occurrence data*.
454 Retrieved from http://rob.schapire.net/papers/nceas.pdf
455 Elith, J., & Leathwick, J. (2017). *Boosted Regression Trees for ecological modeling*. Retrieved
456 from https://cran.r-project.org/web/packages/dismo/vignettes/brt.pdf
457 Fabry, V. J., Seibel, B. A., Feely, R. A., & Orr, J. C. (2008). Impacts of ocean acidification on
458 marine fauna and ecosystem processes. *ICES Journal of Marine Science*, *65*(3), 414–432.
459 https://doi.org/10.1093/icesjms/fsn048
460 Farge, M. (1992). Wavelet Transforms and their Applications to Turbulence. *Annual Review of*

Fluid Mechanics, *24*(1), 395–458. https://doi.org/10.1146/annurev.fl.24.010192.002143

Feng, J., Durant, J. M., Stige, L. C., Hessen, D. O., Hjermann, D. Ø., Zhu, L., … Stenseth, N. C. (2015). Contrasting correlation patterns between environmental factors and chlorophyll levels in the global ocean. *Global Biogeochemical Cycles*, *29*(12), 2095–2107. https://doi.org/10.1002/2015GB005216

Friedman, J. H. (2001). Greedy function approximation: A gradient boosting machine. *The Annals of Statistics*, *29*(5), 1189–1232. https://doi.org/10.1214/aos/1013203451

Friedman, J., Hastie, T., & Tibshirani, R. (2002). Additive logistic regression: a statistical view of boosting (With discussion and a rejoinder by the authors). *The Annals of Statistics*, *28*(2), 337–407. https://doi.org/10.1214/aos/1016218223

Gilgen, H., Ohmura, A., Gilgen, H., & Ohmura, A. (1999). The Global Energy Balance Archive. *Bulletin of the American Meteorological Society*, *80*(5), 831–850. https://doi.org/10.1175/1520-0477(1999)080<0831:TGEBA>2.0.CO;2

Government of Sri Lanka, Ministry of Finance, National Agency for, & Public Private Partnership. (2018). *Framework development and infrastructure financing to support public private partnerships environmental assessment & management framework (EAMF)*. Retrieved from http://documents.worldbank.org/curated/en/972591525333833635/pdf/SFG4315-EA-REVISED-PUBLIC-disclosed-7-24-18.pdf

Han, L., Rundquist, d C., Liu, l L., Fraser, R. N., & Schalles, j F. (1994). The spectral responses of algal chlorophyll in water with varying levels of suspended sediment. *International Journal of Remote Sensing*, *15*(18), 3707–3718. https://doi.org/10.1080/01431169408954353

Han, W., & McCreary, J. P. (2001). Modeling salinity distributions in the Indian Ocean. *Journal of Geophysical Research: Oceans*, *106*(C1), 859–877. https://doi.org/10.1029/2000JC000316

Harrison, W. G. (1992). Regeneration of Nutrients. In *Primary Productivity and Biogeochemical Cycles in the Sea* (pp. 385–407). Boston, MA: Springer US. https://doi.org/10.1007/978-1-4899-0762-2_21

Hendon, H. H., & Salby, M. L. (1994). The Life Cycle of the Madden–Julian Oscillation. *Journal of the Atmospheric Sciences*, *51*(15), 2225–2237. https://doi.org/10.1175/1520-0469(1994)051<2225:TLCOTM>2.0.CO;2

Jana, S., Gangopadhyay, A., Lermusiaux, P. F. J., Chakraborty, A., Sil, S., & Haley, P. J. (2018). Sensitivity of the Bay of Bengal upper ocean to different winds and river input conditions. *Journal of Marine Systems Journal*, (187), 206–222. https://doi.org/10.1016/j.jmarsys.2018.08.001

Jensen, T. G. (2001). Arabian Sea and Bay of Bengal exchange of salt and tracers in an ocean model. *Geophysical Research Letters*, *28*(20), 3967–3970. https://doi.org/10.1029/2001GL013422

Jerlov, N. (1976). *Marine Optics*. *(Elsevier Oceanography Series, 5* (2nd ed., Vol. 14). New york: Elseveir scientific publishing company. https://doi.org/10.1016/S0422-9894(08)70804-3

Jerome H Friedman. (1999). *Greedy Function Approximation: A Gradient Boosting Machine*. Retrieved from https://statweb.stanford.edu/~jhf/ftp/trebst.pdf

Karuppasamy, P. K., Muraleedharan, K. R., Dineshkumar, P. K., & Nair, M. (2010). Distribution of mesopelagic micronekton in the Arabian Sea during the winter monsoon. *Indian Journal*

of Marine Sciences, *39*(2), 227–237.

Kendall, M. G. (1938). A New Measure of Rank Correlation. *Biometrika*, *30*(1/2), 81. https://doi.org/10.2307/2332226

Kessler, A., & Jaeger, L. (1999). Long-term changes in net radiation and its components above a pine forest and a grass surface in Germany. *International Journal of Climatology*, *19*(2), 211–226. https://doi.org/10.1002/(SICI)1097-0088(199902)19:2<211::AID-JOC351>3.0.CO;2-1

Kirk, J. T. O. (1994). *Light and photosynthesis in aquatic ecosystems*. New york: Cambridge University Press.

Kirk, J. T. O. (2011). *Light and photosynthesis in aquatic ecosystems* (3rd ed.). New york: Cambridge University Press. Retrieved from www.cambridge.org/9780521151757

Kong, F., Dong, Q., Xiang, K., Yin, Z., Li, Y., Liu, J., … Liu, J. (2019). Spatiotemporal Variability of Remote Sensing Ocean Net Primary Production and Major Forcing Factors in the Tropical Eastern Indian and Western Pacific Ocean. *Remote Sensing*, *11*(4), 391. https://doi.org/10.3390/rs11040391

Kraemer, B. M., Mehner, T., & Adrian, R. (2017). Reconciling the opposing effects of warming on phytoplankton biomass in 188 large lakes. *Scientific Reports*, *7*(1), 10762. https://doi.org/10.1038/s41598-017-11167-3

Krishna, M. S., Prasad, V. R., Sarma, V. V. S. S., Reddy, N. P. C., Hemalatha, K. P. J., & Rao, Y. V. (2015). *Fluxes of dissolved organic carbon and nitrogen to the Northern Indian Ocean from the Indian monsoonal rivers*. *J. Geophys. Res. (G: Biogeosciences)* (Vol. 120). Retrieved from http://drs.nio.org/drs/bitstream/handle/2264/4888/J_Geophys_Res_G_120_2067a.pdf?seque

nce=1&isAllowed=y

Kug, J.-S., & Kang, I.-S. (2006). Interactive Feedback between ENSO and the Indian Ocean. *Journal of Climate*, *19*(9), 1784–1801. https://doi.org/10.1175/JCLI3660.1

Kumar, G. S., Prakash, S., Ravichandran, M., & Narayana, A. C. (2016). Trends and relationship between chlorophyll-a and sea surface temperature in the central equatorial Indian Ocean. *Remote Sensing Letters*, *7*(11), 1093–1101. https://doi.org/10.1080/2150704X.2016.1210835

Kutser, T., Herlevi, A., Kallio, K., & Arst, H. (2001). A hyperspectral model for interpretation of passive optical remote sensing data from turbid lakes. *Undefined*. Retrieved from https://www.semanticscholar.org/paper/A-hyperspectral-model-for-interpretation-of-passive-Kutser-Herlevi/bac92f316d5ab855656c9016c00810707c7ab475

Lagerloef, G. S. E. (2002). Introduction to the special section: The role of surface salinity on upper ocean dynamics, air-sea interaction and climate. *Journal of Geophysical Research: Oceans*, *107*(C12), SRF 1-1-SRF 1-2. https://doi.org/10.1029/2002JC001669

Levitus, S., Conkright, M. E., Reid, J. L., Najjar, R. G., & Mantyla, A. (1993). Distribution of nitrate, phosphate and silicate in the world oceans. *Progress in Oceanography*, *31*(3), 245–273. https://doi.org/10.1016/0079-6611(93)90003-V

Lin, S., Qi, J., Jones, J. R., & Stevenson, R. J. (2018). Effects of sediments and coloured dissolved organic matter on remote sensing of chlorophyll-a using Landsat TM/ETM+ over turbid waters. *International Journal of Remote Sensing*, *39*(5), 1421–1440. https://doi.org/10.1080/01431161.2017.1404164

Luis, A. J., & Kawamura, H. (2004). Air-sea interaction, coastal circulation and primary production in the eastern Arabian Sea: A review. *Journal of Oceanography*, *60*(3), 205–

218. https://doi.org/10.1023/B:JOCE.0000038327.33559.34

Lumban-Gaol, J., Leben, R. R., Vignudelli, S., Mahapatra, K., Okada, Y., Nababan, B., … Syahdan, M. (2015). Variability of satellite-derived sea surface height anomaly, and its relationship with Bigeye tuna (Thunnus obesus) catch in the Eastern Indian Ocean. *European Journal of Remote Sensing*, *48*(1), 465–477. https://doi.org/10.5721/EuJRS20154826

Maraun, D., & Kurths, J. (2004). *Cross wavelet analysis: significance testing and pitfalls Nonlinear Processes in Geophysics Cross wavelet analysis: significance testing and pitfalls*. *European Geosciences Union (EGU)* (Vol. 11). Retrieved from https://hal.archives-ouvertes.fr/hal-00302384

Mateo, I., & Hanselman, D. (2014). A Comparison of Statistical Methods to Standardize Catch-Per-Unit-Effort of the Alaska Longline Sablefish Fishery. *U.S.Dep.Commer.,NOAA Tech. Memo. NMFS-AFSC-269*, (February), 1–71. Retrieved from http://docs.lib.noaa.gov/noaa_documents/NMFS/AFSC/TM_AFSC/TM_NMFS_AFSC_269.pdf

Narvekar, J., & Kumar, S. P. (2014). Mixed layer variability and chlorophyll a biomass in the Bay of Bengal. *Biogeosciences*, *11*, 3819–3843. https://doi.org/10.5194/bg-11-3819-2014

Nieto, K., & Mélin, F. (2017). Variability of chlorophyll-a concentration in the Gulf of Guinea and its relation to physical oceanographic variables. *Progress in Oceanography*, *151*, 97–115. https://doi.org/10.1016/j.pocean.2016.11.009

Prakash, S., & Ramesh, R. (2007). *Is the Arabian Sea getting more productive?* Retrieved from http://www.indiaenvironmentportal.org.in/files/cl7.pdf

Rath, S., Vinaychandran, P. N., Behara, A., & Neema, C. P. (2017). Dynamics of Summer

576 Monsoon Current around Sri Lanka. *Atmospheric and Oceanic Physics*. Retrieved from
577 https://arxiv.org/pdf/1711.03311.pdf
578 Sarangi, R. K., & Devi, K. N. (2017). Space-based observation of chlorophyll, sea surface
579 temperature, nitrate, and sea surface height anomaly over the Bay of Bengal and Arabian
580 Sea. *Advances in Space Research*, *59*(1), 33–44. https://doi.org/10.1016/j.asr.2016.08.038
581 Sathyendranath, S., Gouveia, A. D., Shetye, S. R., Ravindran, P., & Platt, T. (1991). Biological
582 control of surface temperature in the Arabian Sea. *Nature*, *349*(6304), 54–56.
583 https://doi.org/10.1038/349054a0
584 Schott, F. A., Dengler, M., & Schoenefeldt, R. (2002). The shallow overturning circulation of the
585 Indian Ocean. *Progress in Oceanography*, *53*(1), 57–103. https://doi.org/10.1016/S0079-
586 6611(02)00039-3
587 Schott, F. A., & McCreary, J. P. (2001). The monsoon circulation of the Indian Ocean. *Progress*
588 *in Oceanography*, *51*(1), 1–123. https://doi.org/10.1016/S0079-6611(01)00083-0
589 Scott C. Doney, Ruckelshaus, M., Duffy, J. E., Barry, J. P., Chan, F., English, C. A., … Talley,
590 L. D. (2012). Climate change impacts on marine ecosystems. *Annual Review OfMarine*
591 *Science*, *2012*(4), 11–37.
592 Strutton, P. G., Coles, V. J., Hood, R. R., Matear, R. J., Mcphaden, M. J., & Phillips, H. E.
593 (2015). Biogeochemical variability in the central equatorial Indian Ocean during the
594 monsoon transition. *Biogeosciences*, *12*, 2367–2382. https://doi.org/10.5194/bg-12-2367-
595 2015
596 Tang, D., Kawamura, H., & Luis, A. J. (2002). *Short-term variability of phytoplankton blooms*
597 *associated with a cold eddy in the northwestern Arabian Sea*. Retrieved from
598 www.elsevier.com/locate/rse

599 Tang, D. L., Kawamura, H., & Luis, A. J. (2002). Short-term variability of phytoplankton
600 blooms associated with a cold eddy in the northwestern Arabian Sea. *Remote Sensing of*
601 *Environment*, *81*(1), 82–89. https://doi.org/10.1016/S0034-4257(01)00334-0
602 Tang, D., & Pan, B. (2011). *Remote sensing of the changing oceans*. Springer. Retrieved from
603 http://lib1.org/_ads/6275672CB62DA48988F005D29B48049C
604 Torrence, C., & Compo, G. P. (1998). A Practical Guide to Wavelet Analysis. *Bulletin of the*
605 *American Meteorological Society*, *79*(1), 61–78. https://doi.org/10.1175/1520-
606 0477(1998)079<0061:APGTWA>2.0.CO;2
607 Valadão, C. E. A., Carvalho, L. M. V., Lucio, P. S., & Chaves, R. R. (2017). Impacts of the
608 Madden-Julian oscillation on intraseasonal precipitation over Northeast Brazil.
609 *International Journal of Climatology*, *37*(4), 1859–1884. https://doi.org/10.1002/joc.4818
610 Vernet, M., Wendy, A. K., Lynn, R. Y., Alexander, T. L., Robin, M. R., Langdon, B. Q., &
611 Christian, H. F. (2012). Primary production throughout austral fall, during a time of
612 decreasing daylength in the western Antarctic Peninsula. *Marine Ecology Progress Series*,
613 *452*(April 2015), 45–61. https://doi.org/10.3354/meps09704
614 Vinayachandran, P. N., Murty, V. S. N., & Ramesh Babu, V. (2002). Observations of barrier
615 layer formation in the Bay of Bengal during summer monsoon. *Journal of Geophysical*
616 *Research: Oceans*, *107*(C12), SRF 19-1-SRF 19-9. https://doi.org/10.1029/2001JC000831
617 Waliser, D. E., Murtugudde, R., Strutton, P., & Li, J.-L. (2005). Subseasonal organization of
618 ocean chlorophyll: Prospects for prediction based on the Madden-Julian Oscillation.
619 *Geophysical Research Letters*, *32*(23), L23602. https://doi.org/10.1029/2005GL024300
620 Weisberg, R. H., & Wang, C. (1997). Slow Variability in the Equatorial West-Central Pacific in
621 Relation to ENSO. *Journal of Climate*, *10*(8), 1998–2017. https://doi.org/10.1175/1520-

622 0442(1997)010<1998:SVITEW>2.0.CO;2

623 Wiggert, J. D., Murtugudde, R. G., & Christian, J. R. (2006). Annual ecosystem variability in the

624 tropical Indian Ocean: Results of a coupled bio-physical ocean general circulation model.

625 *Deep Sea Research Part II: Topical Studies in Oceanography*, *53*(5–7), 644–676.

626 https://doi.org/10.1016/J.DSR2.2006.01.027

627

Figure 1(on next page)

Figure 1 : Study area in blue color lied in 720 E, 00N and 98.50E, 220N

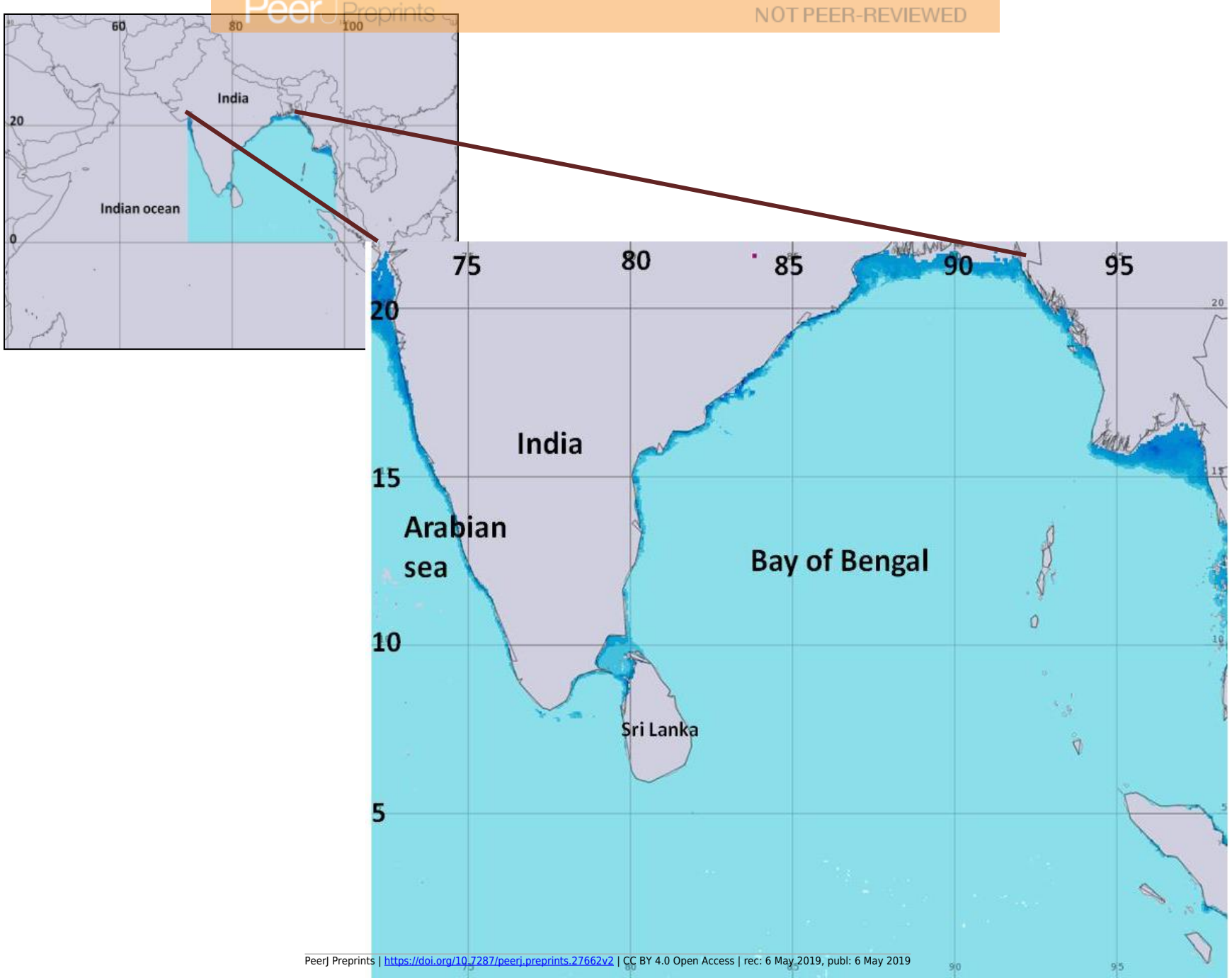

PeerJ Preprints | https://doi.org/10.7287/peerj.preprints.27662v2 | CC BY 4.0 Open Access | rec: 6 May 2019, publ: 6 May 2019

Figure 2(on next page)

Figure 2 : The monthly mean variability of the Chl-a and the influencing factors. A:Chl-a, Surface emissivity, Diffuse attenuation coefficient, PAR,SST, Nitrate; B: Chl-a, Wind speed, Eastward wind component, Black carbon concentration, Sea surface sa

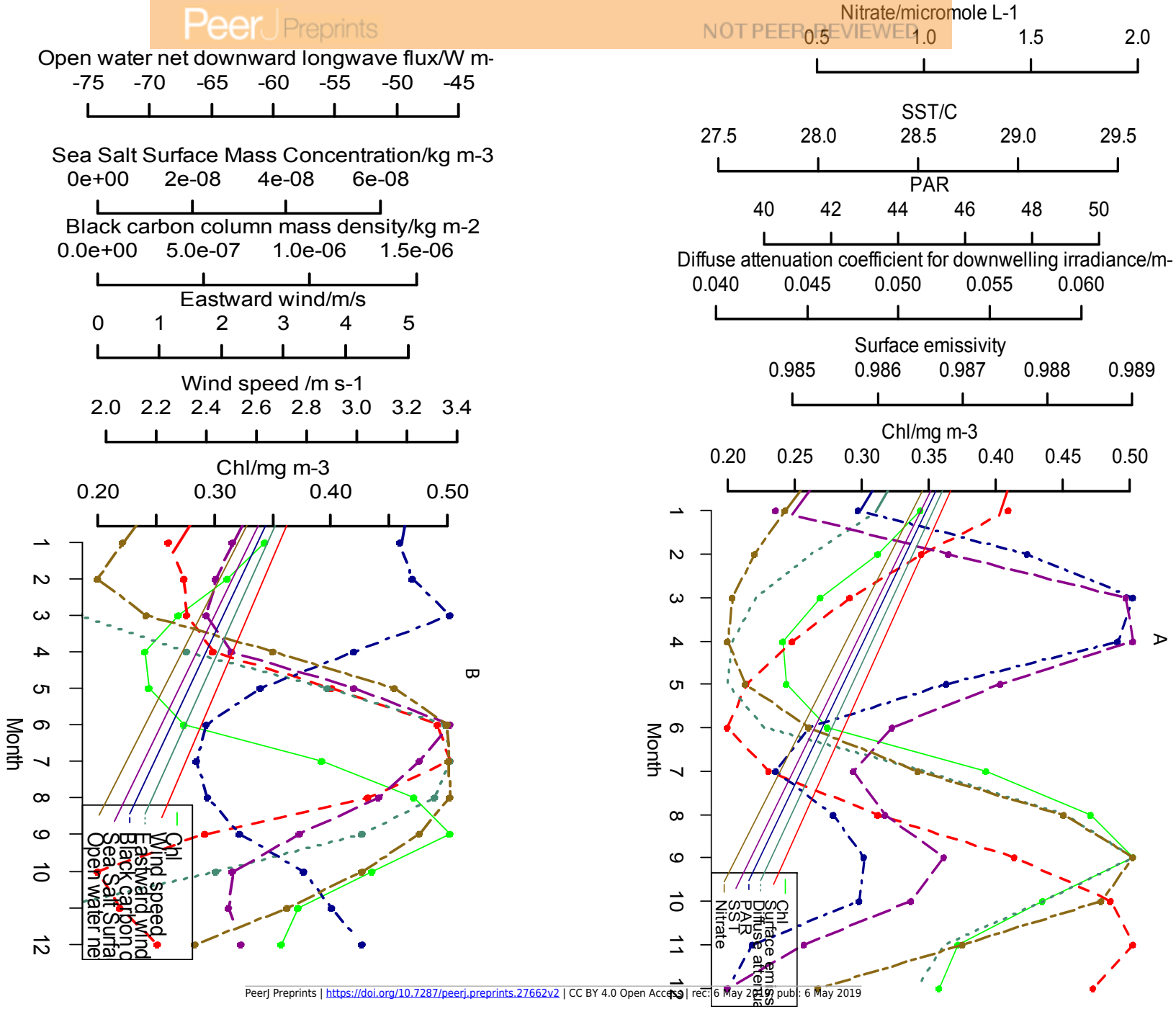

PeerJ Preprints | https://doi.org/10.7287/peerj.preprints.27662v2 | CC BY 4.0 Open Acce | rec: 6 May 2 pub: 6 May 2019

Figure 3(on next page)

Figure 3 . Exponent wavelet coherences among Chlorophyll and influential variables from 2002-2018. The horizontal axis is the 17 years of monthly record beginning from September 2002.

The Cone of Influence defines the areas that are not influenced by edge effects of the wavelet spectra. Colours indicate the strength of the coherence, Yellow to red areas demonstrates the significant correlation at the 95% level against red noise. Directions of the arrows indicate the degree to which the chl-a and other variable series are in phase or outphase. Right arrows indicate they are completely inphase, left indicate they are completely outphase (180° phase angle), and down arrows indicate chl-a lags influencing variable by 90° (one fourth of the cycle at that period). A phase-difference between 0 and ± π /2 indicates the variables are in-phase (or positively related) while a phase difference of absolute magnitude greater than π /2 indicates an out of phase (or negative) relationship.

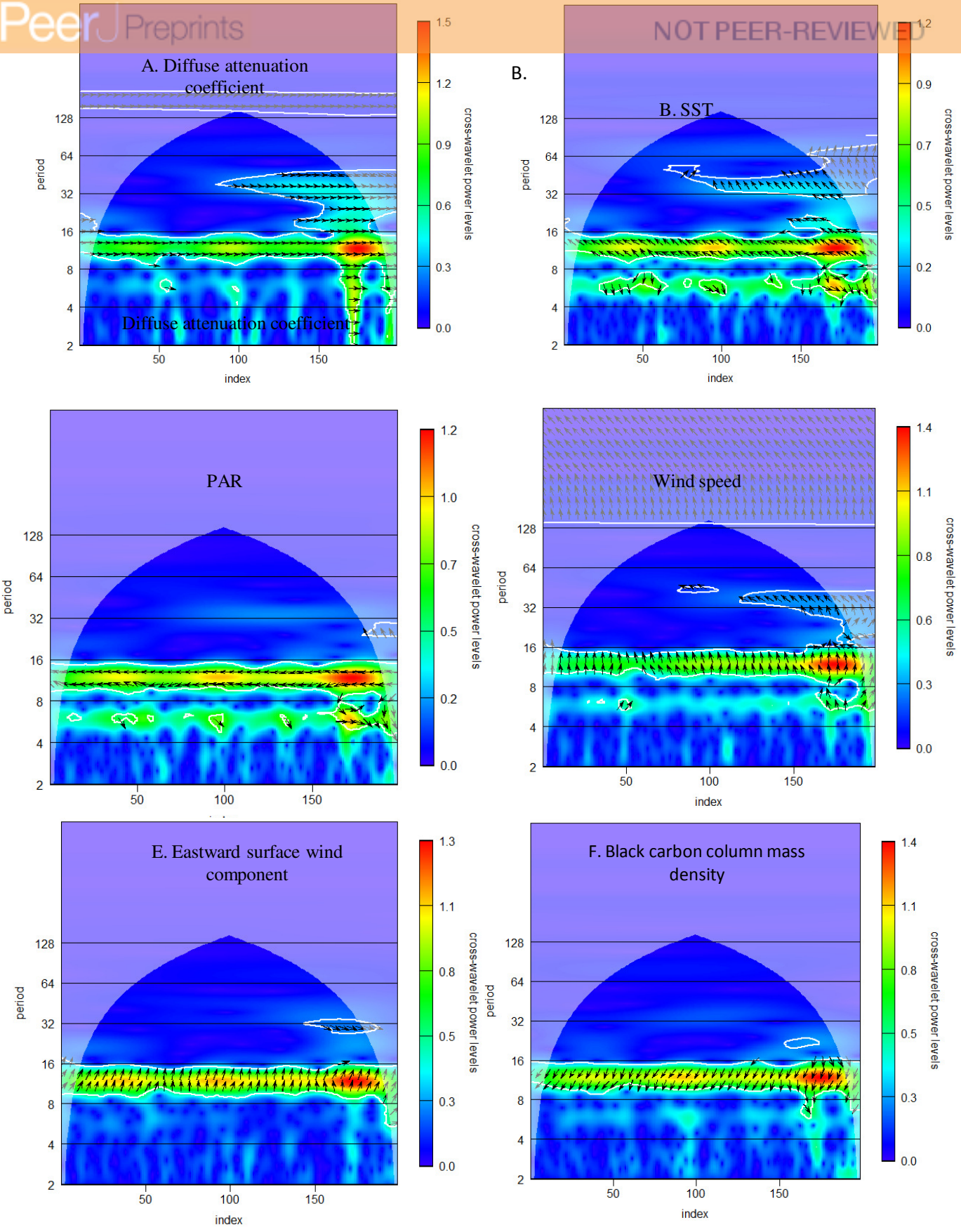

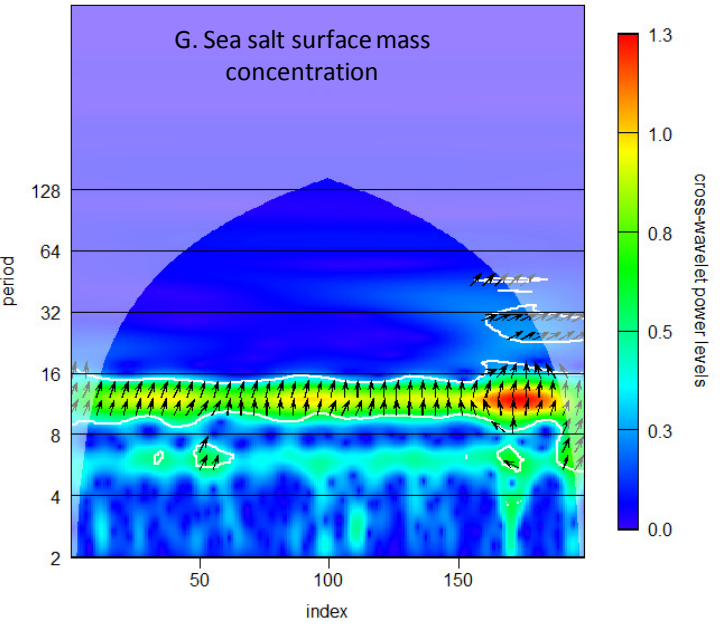
G. Sea salt surface mass concentration
period
128
64
32
16
8
4
2
50
100
150
index
1.3
1.0
0.8
0.5
0.3
0.0
cross-wavelet power levels

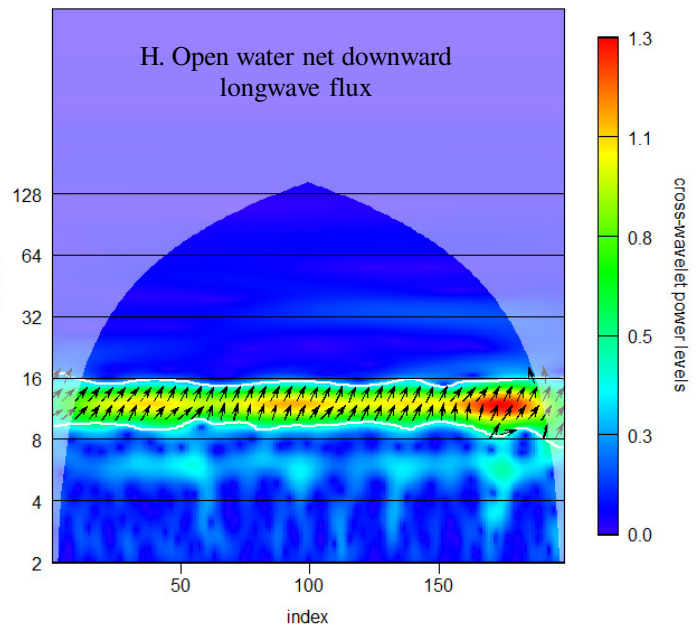
H. Open water net downward longwave flux
period
128
64
32
16
8
4
2
50
100
150
index
1.3
1.1
0.8
0.5
0.3
0.0
cross-wavelet power levels

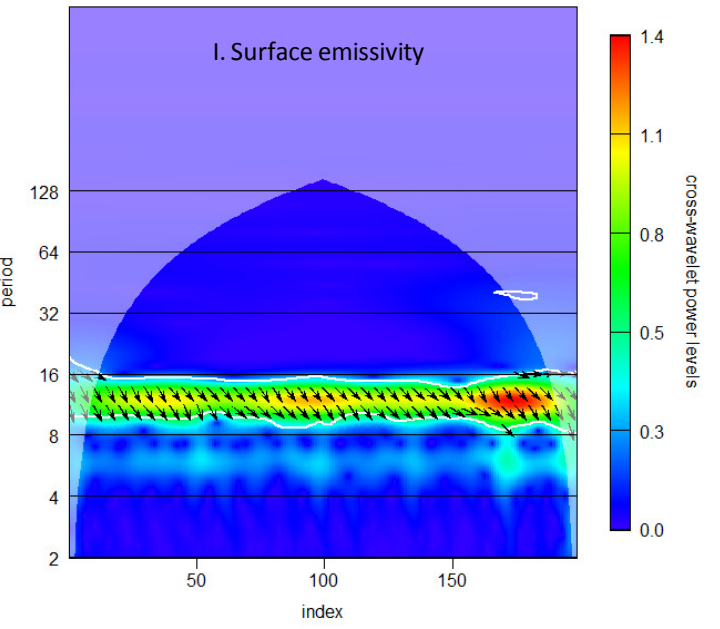
I. Surface emissivity
period
128
64
32
16
8
4
2
50
100
150
index
1.4
1.1
0.8
0.5
0.3
0.0
cross-wavelet power levels

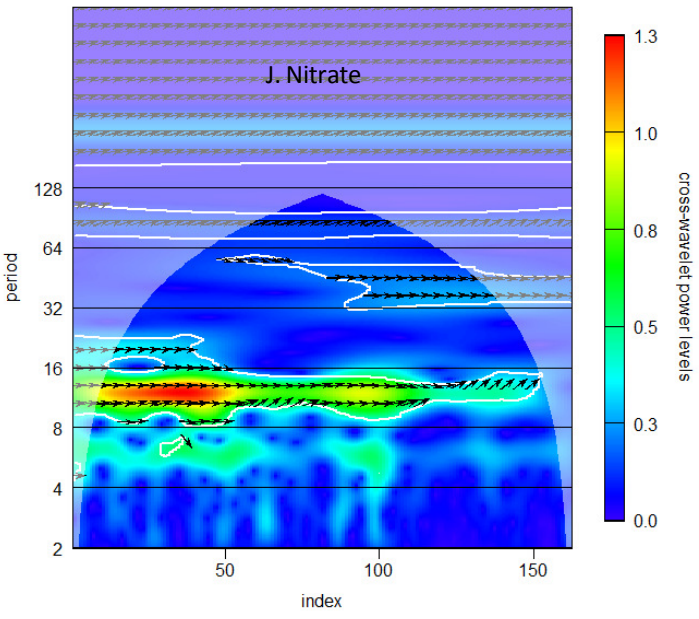
J. Nitrate
period
128
64
32
16
8
4
2
50
100
150
index
1.3
1.0
0.8
0.5
0.3
0.0
cross-wavelet power levels

Figure 4(on next page)

Figure 4 . The BRT model holdout deviance vs no of trees.

The lowest predictive deviance achieved for each panel is indicated by a dotted horizontal line; the line for learning rate achieving the minimum is shown in bold line.

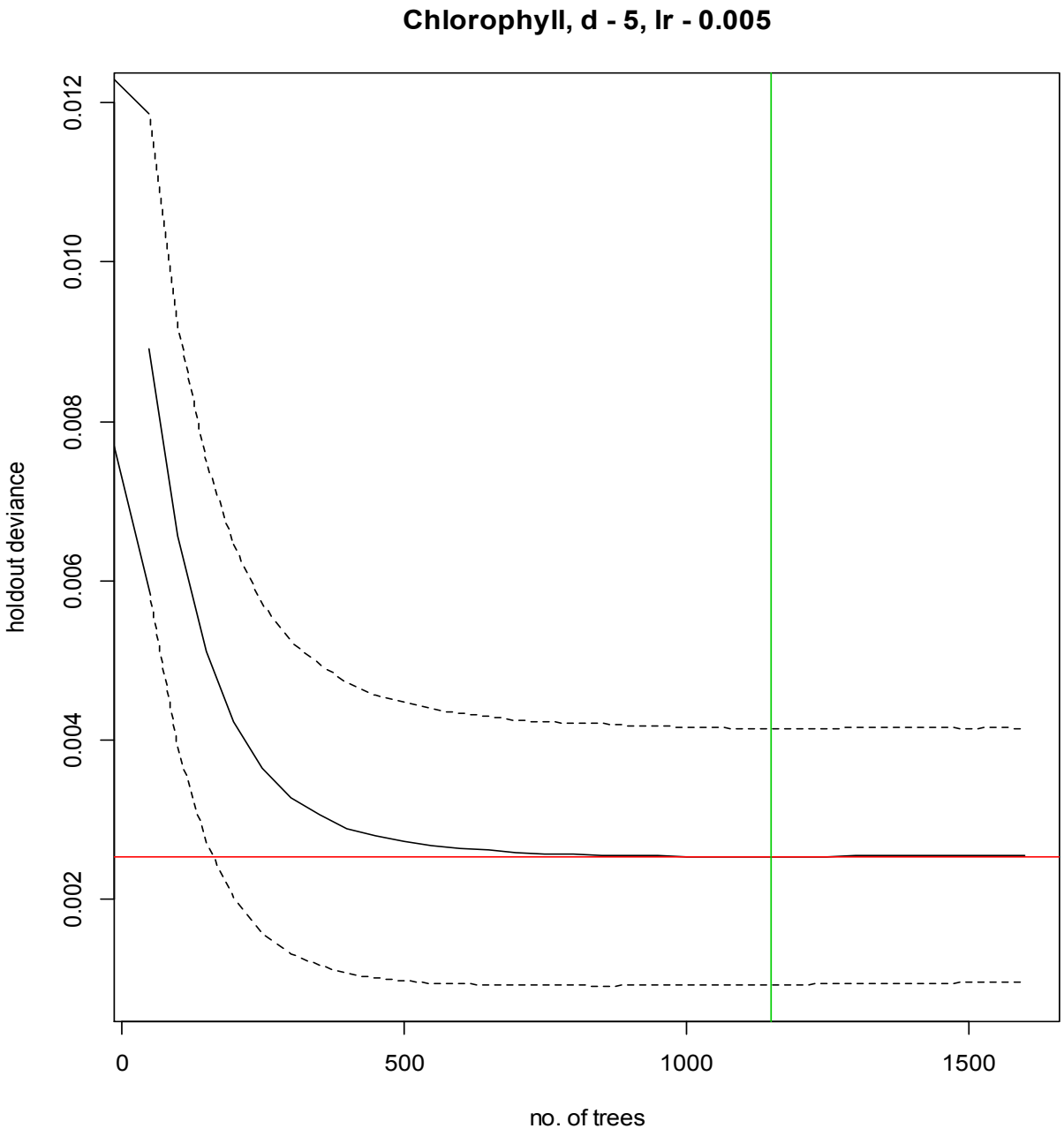

PeerJ Preprints | https://doi.org/10.7287/peerj.preprints.27662v2 | CC BY 4.0 Open Access | rec: 6 May 2019, publ: 6 May 2019

Figure 5(on next page)

Figure 5 . Relative influence of variables on Chl-a according to BRT

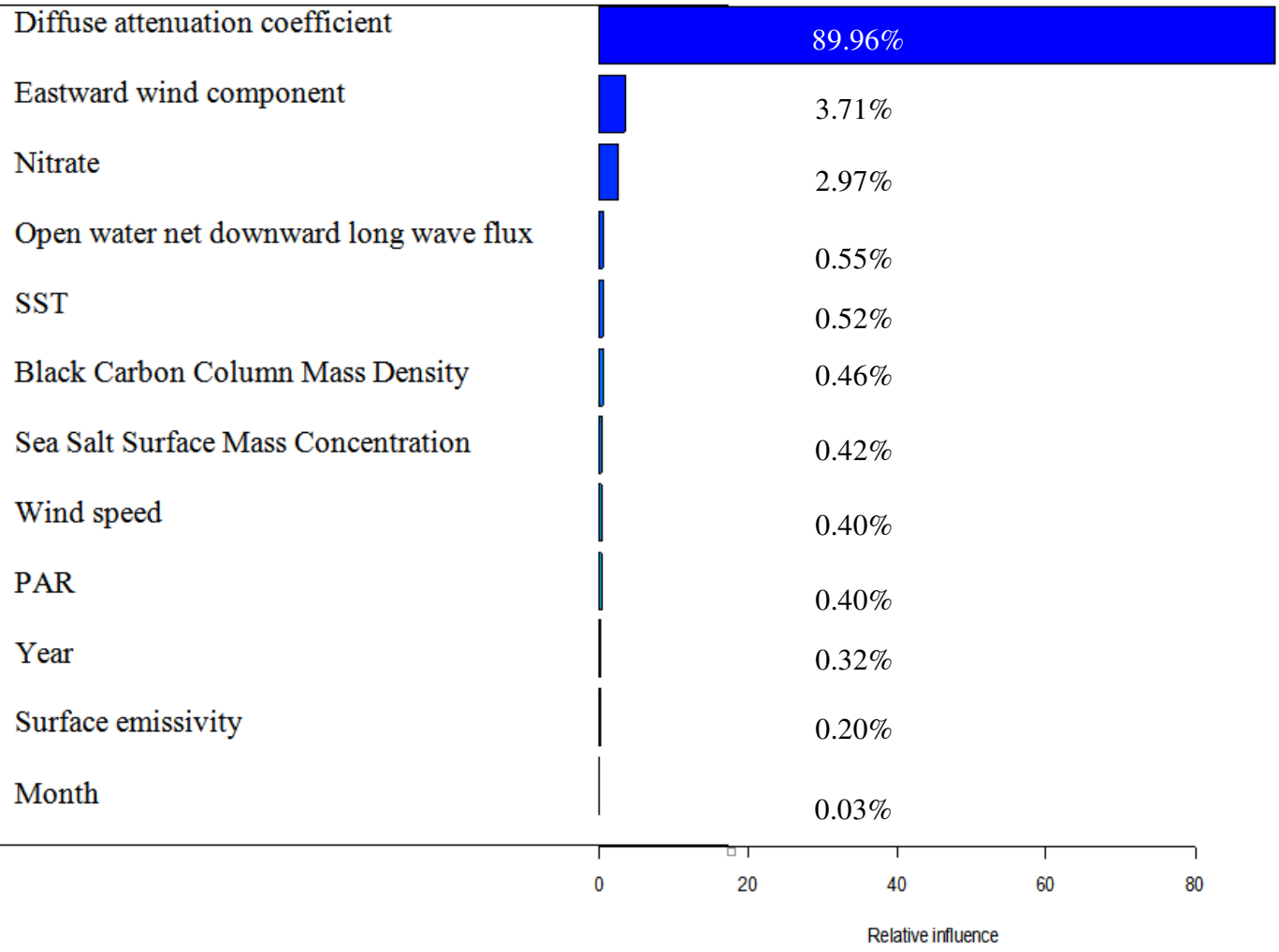
Diffuse attenuation coefficient
89.96%
Eastward wind component
3.71%
Nitrate
2.97%
Open water net downward long wave flux
0.55%
SST
0.52%
Black Carbon Column Mass Density
0.46%
Sea Salt Surface Mass Concentration
0.42%
Wind speed
0.40%
PAR
0.40%
Year
0.32%
Surface emissivity
0.20%
Month
0.03%
0
20
40
60
80
Relative influence

Figure 6(on next page)

Figure 6 . Partial dependence plots for the BRT. Each plot shows the relationship of chl (response variable) to the individual variable after accounting for the effects of all the predictor variables in the final model

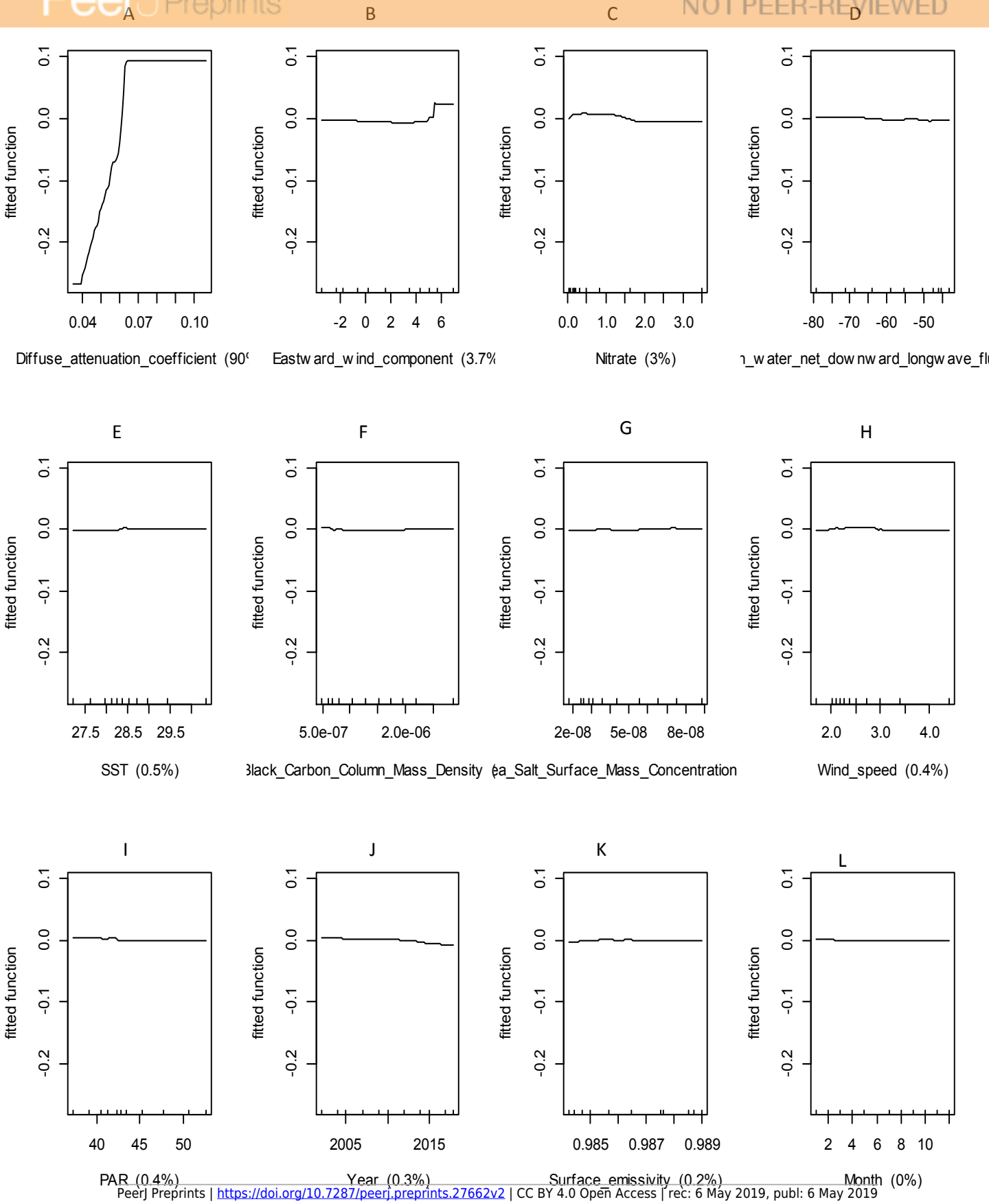

PeerJ Preprints | https://doi.org/10.7287/peerj.preprints.27662v2 | CC BY 4.0 Open Access | rec: 6 May 2019, publ: 6 May 2019

Figure 7 (on next page)

Figure 7 . weighted mean of fitted values in relation to each non-factor predictor

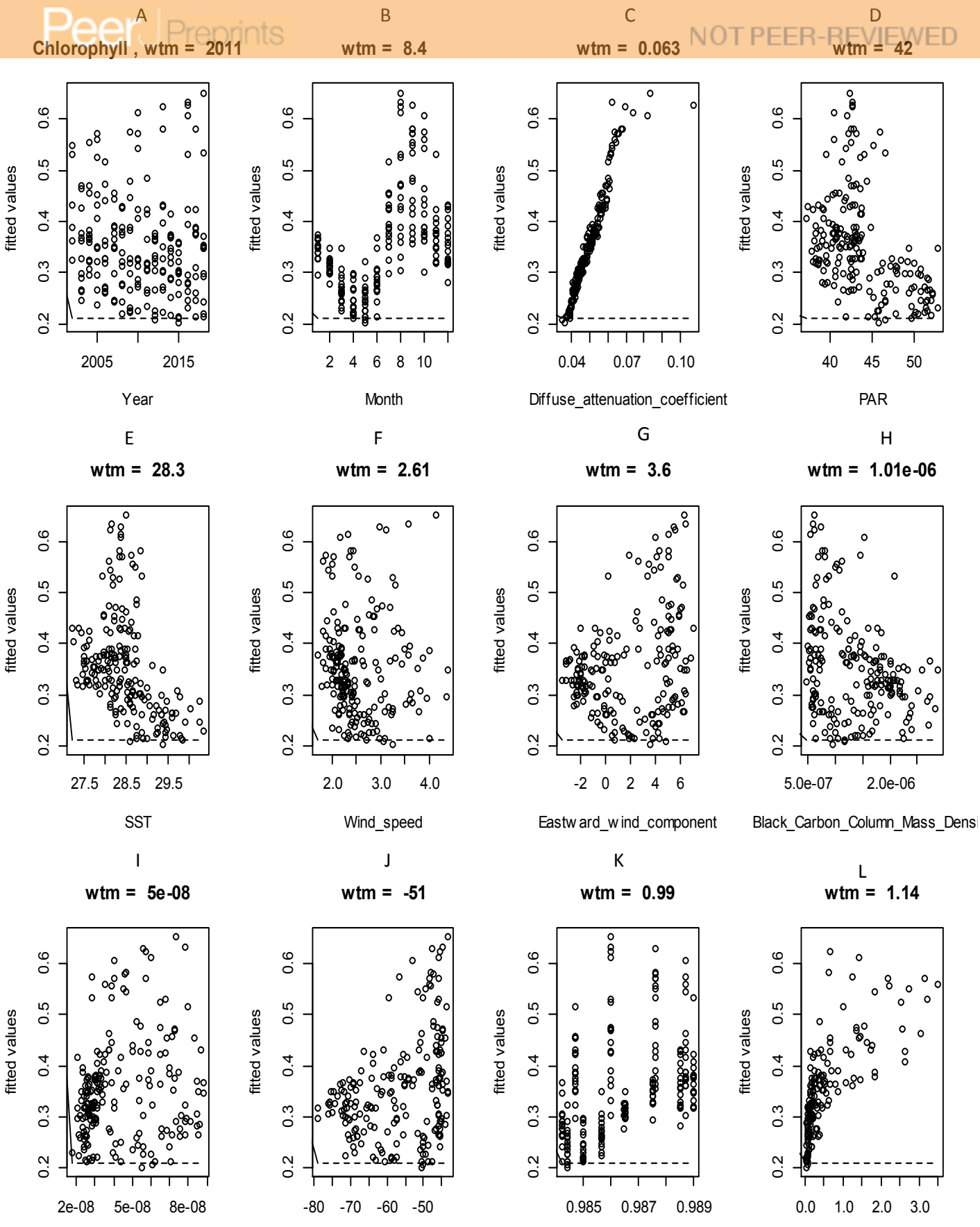

PeerJ Preprints | https://doi.org/10.7287/peerj.preprints.27662v2 | CC BY 4.0 Open Access | rec: 6 May 2019, publ: 6 May 2019

Figure 8(on next page)

Figure 8 .The relationship between the influencing variable and the mapping function f(x) of Chl-a

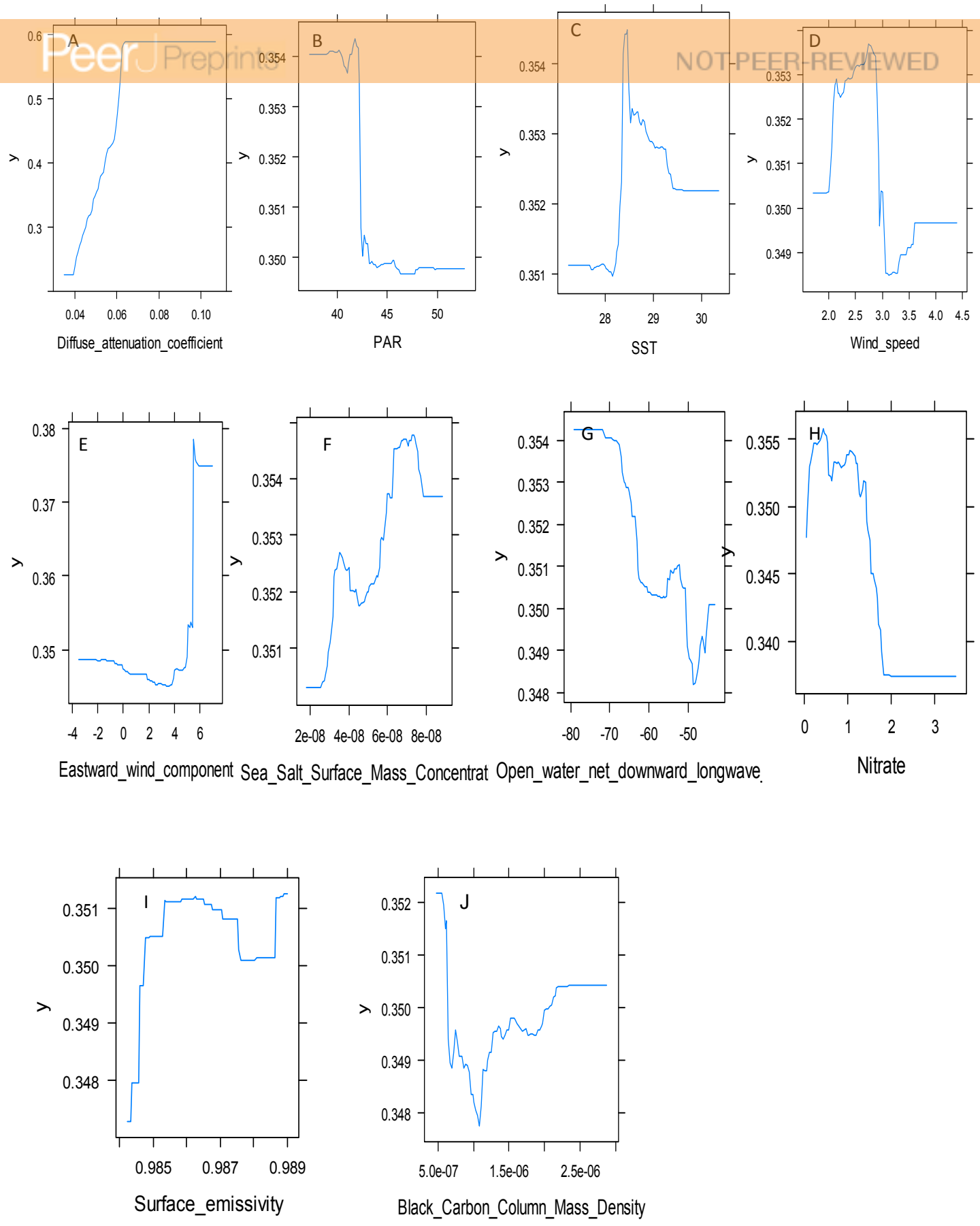

Figure 9(on next page)

Figure 9 : Seasonal variations of the important predictor variables

(A:December - February, B: March-May, C: June-August, D:September-November)

Diffuse attenuation coefficient

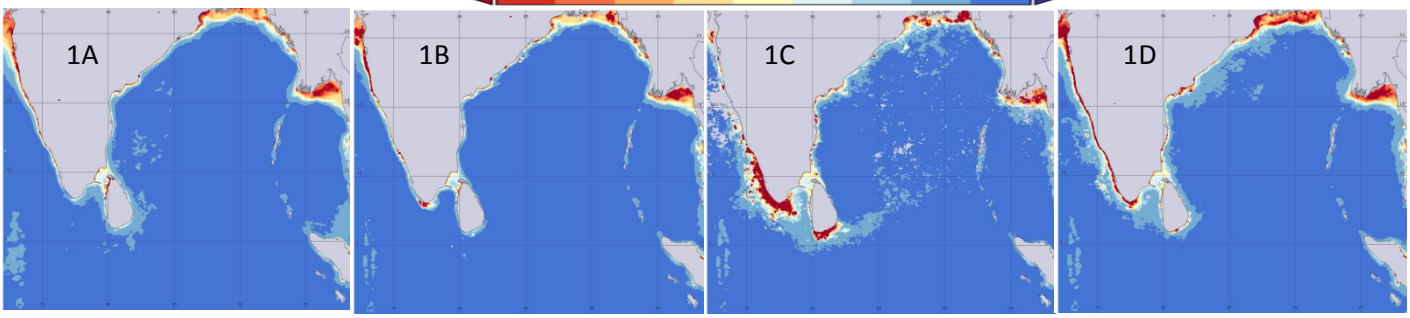

Eastward wind component

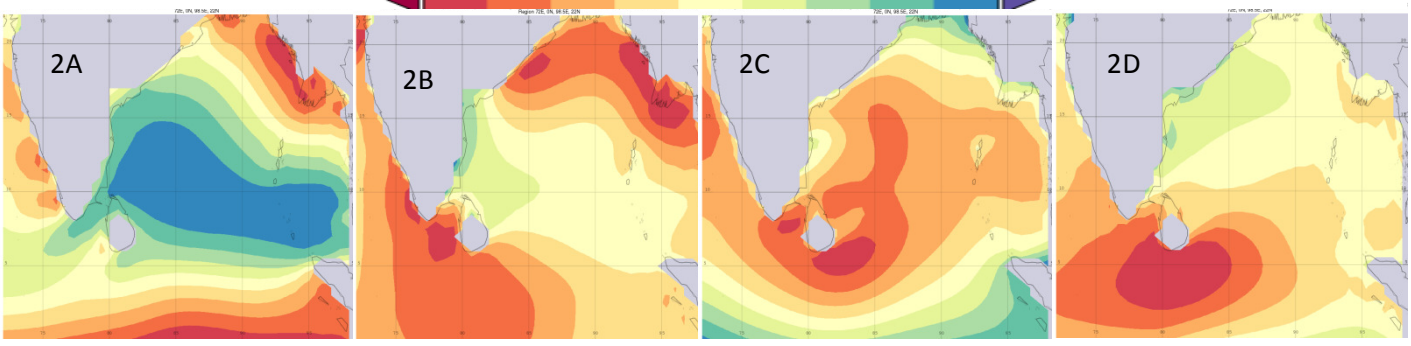

Nitrate

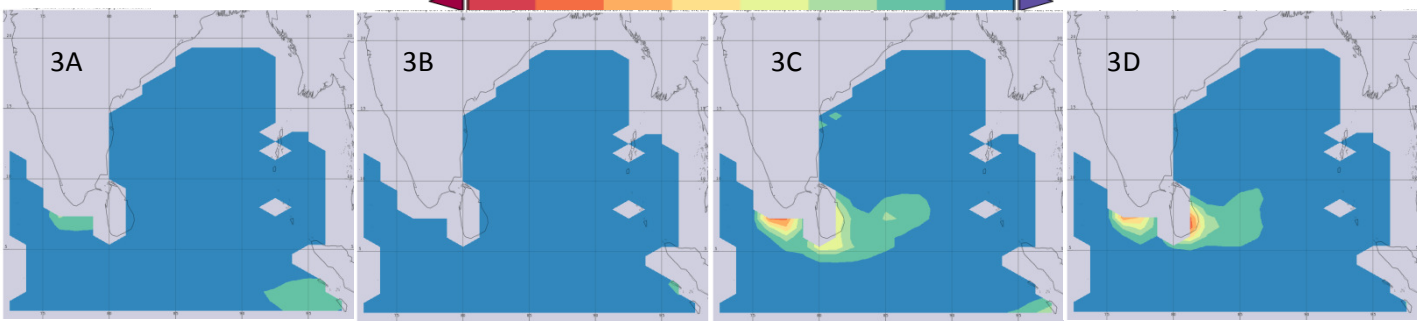

Open water net downward long wave radiation

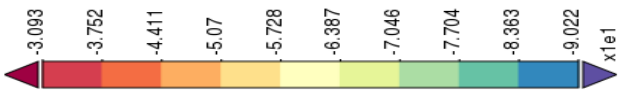

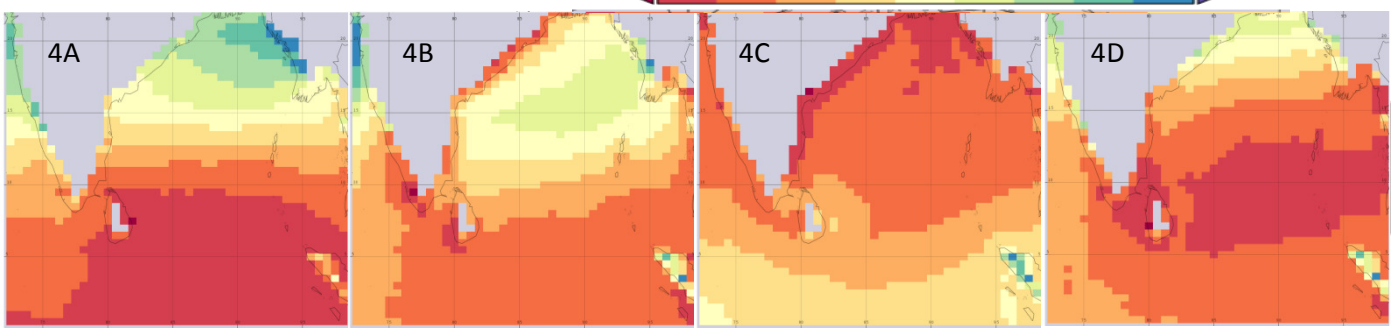

SST

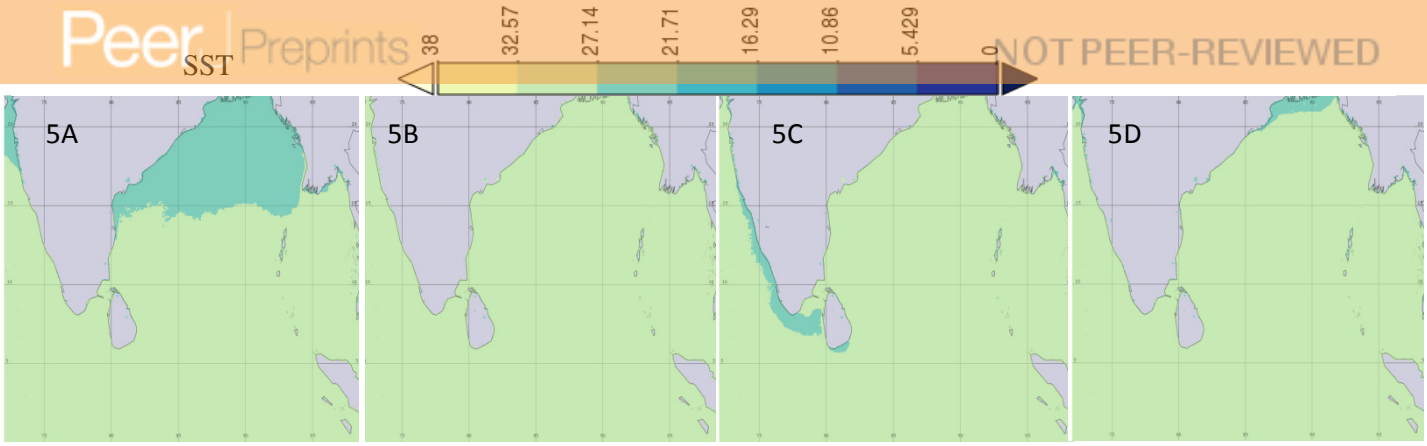

Chl-a

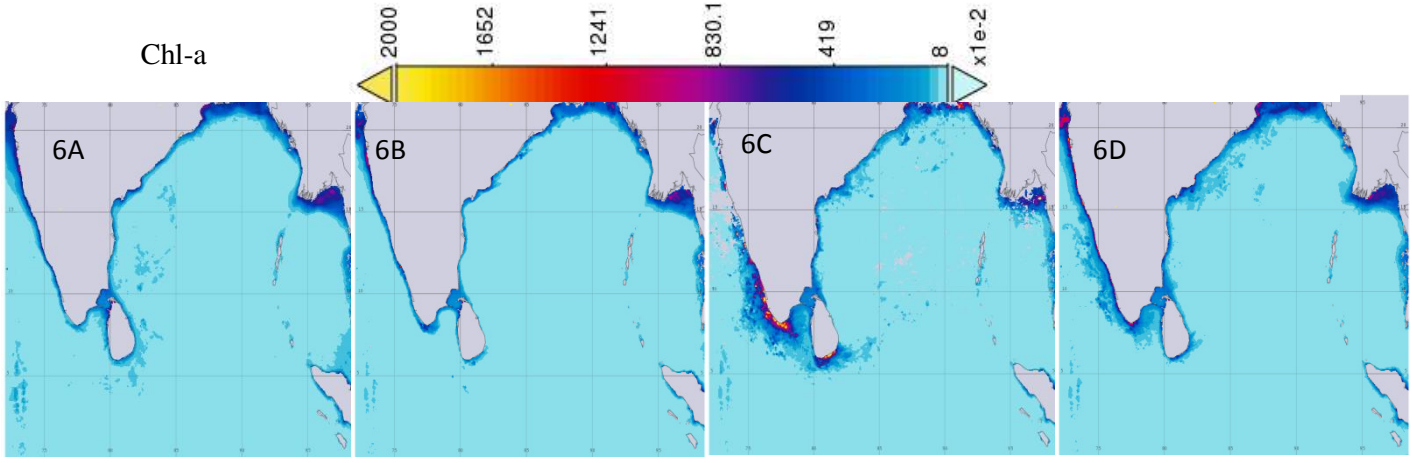

Table 1(on next page)

Table 1 : Standard deviations of the data sets of the variables for 17 years

1

Month	Wind speed_ms-1	Eastward wind component_ms-1	Black Carbon Column Mass Density_kg m-2	Sea Salt Surface Mass Concentration_kg m-3	Open water net downward longwave flux_W m-2	Surface emissivity	Chlorophyll_mg m-3	Diffuse attenuation coefficient	PAR_Einstein m^-2 day^-1	SST/C	Nitrate_micromole/L
1	0.136584	0.518457	6.61E-07	3.58E-09	3.074785	3.04E-07	0.02451	0.002272	0.857566	0.238596	0.22781
2	0.121934	0.574535	6.05E-07	4.09E-09	4.666203	6.15E-06	0.016366	0.001543	1.305851	0.272649	0.130863
3	0.124211	0.628681	6.17E-07	3.18E-09	3.401756	1.12E-16	0.033587	0.002466	1.339659	0.304124	0.049041
4	0.23746	0.880342	3.39E-07	7.17E-09	3.297025	2.25E-16	0.030325	0.002444	1.180281	0.419891	0.045254
5	0.224524	0.795107	1.93E-07	1.2E-08	2.67719	2.23E-07	0.041183	0.003064	1.296965	0.31888	0.155564
6	0.404756	0.751985	1.32E-07	8.03E-09	1.567404	3.66E-07	0.035445	0.002894	1.320166	0.255882	0.375145
7	0.527142	0.531893	1.01E-07	9.01E-09	1.832075	3.39E-07	0.059568	0.004736	0.996373	0.195472	0.688112
8	0.424981	0.565545	1.45E-07	7.03E-09	1.15554	0	0.124896	0.009716	0.932357	0.167753	1.207734
9	0.274786	0.565934	2.68E-07	6.46E-09	1.765892	6.75E-16	0.177968	0.012981	1.409933	0.257784	1.359942
10	0.137613	1.285265	5.03E-07	7.62E-09	2.9888	2.25E-16	0.109651	0.00807	1.365595	0.191154	1.502404
11	0.133549	1.146751	4.36E-07	5.39E-09	2.827924	5.62E-16	0.044419	0.003815	1.243705	0.25459	1.288086
12	0.129899	0.877466	5.27E-07	4.63E-09	3.040033	4.5E-16	0.045559	0.004184	1.067088	0.225655	0.62403

2

3

4

5

6

7

8

Table 2(on next page)

Table 2 : Kendall's rank correlation results declaration

1

2

Variable	Kendall's rank correlations	Chi Sq	P
Diffuse attenuation coefficient	0.9929	391.1953	<0.0001
PAR	0.266	104.7891	1.00
SST	0.2532	99.7513	1.00
Wind speed	0.4043	159.296	0.98
Eastward wind component	0.5901	232.4897	0.04
Nitrate	0.9118	293.5874	<0.0001
Black carbon column mass density	0.3623	142.7583	1.00
Sea Salt Surface Mass Concentration	0.6044	238.1378	0.02
Open water net downward longwave flux	0.64	252.1486	0.00
Surface emissivity	0.7658	301.737	<0.0001